DOI: 10.1002/cbic.200800437

Inhibition of *Mycobacterium tuberculosis* Pantothenate Synthetase by Analogues of the Reaction Intermediate

Alessio Ciulli,*[a] Duncan E. Scott,[a] Michiyo Ando,[a, c] Fernando Reyes,[a, d] S. Adrian Saldanha,[a, e] Kellie L. Tuck,[a, f] Dimitri Y. Chirgadze,[b] Tom L. Blundell,[b] and Chris Abell*[a]

Mycobacterium tuberculosis, the causative agent of tuberculosis (TB), infects approximately two billion people worldwide, and an estimated nine million of these develop TB each year.[1,2] TB is currently the leading cause of infectious disease mortality in the world by a bacterial pathogen, and claimed an estimated 1.7 million deaths in 2006.[3] As a result of the increasing manifestation of multiple-drug-resistant strains of *M. tuberculosis* and of the limitations of the current anti-TB therapies, the development of safe and effective new drugs with novel modes of action is urgently needed.[4]

Pantothenate (vitamin B_5) is the essential precursor to coenzyme A and acyl carrier proteins. The de novo biosynthetic pathway to pantothenate is present in many bacteria, fungi and plants and comprises four enzymes, encoded by *panB*, *panE*, *panD* and *panC*.[5] Bioinformatics analyses have identified this pathway as a potential target for antimicrobial agents.[6] The absence of each enzyme in mammals further suggests that inhibitors could be selective with a reduced risk of side effects. Crucially, genetic studies have shown that a pantothenate auxotroph of *M. tuberculosis* defective in the *panC* and *panD* genes fails to establish virulence in a mouse model of infection.[7] An attenuated strain of *M. tuberculosis* that deletes both *panCD* and the primary attenuating mutations of the bacille Calmette–Guérin (BCG) strain is now being considered as a human vaccine candidate for protection against TB.[8] A potential pitfall of inhibiting pantothenate biosynthesis as a general antimicrobial strategy is the ability of several bacteria, including *Escherichia coli*, to acquire pantothenate from the environment through pantothenate permease (*panF*).[9] However, to date, no *panF* homologues have been identified in the *M. tuberculosis* genome. Furthermore, it has been suggested that rescue of pantothenate through a putative salvage pathway might only be sufficient for *M. tuberculosis* to survive but not to cause disease.[7,10] The pantothenate pathway is therefore an attractive target for inhibitors that could provide lead compounds for novel antitubercular drugs.

We have chosen to target *M. tuberculosis* pantothenate synthetase (PS, E.C. 6.3.2.1), the product of the *panC* gene. Pantothenate synthetase catalyzes the final step in the biosynthesis of pantothenate through a Bi Uni Uni Bi Ping Pong kinetic mechanism that consists of two consecutive steps.[11,12] The first reaction, which occurs upon sequential binding of ATP and pantoate, is the Mg^{2+}-dependent formation of a tightly-bound pantoyl adenylate intermediate (**1**) followed by the release of pyrophosphate. In the second reaction, nucleophilic attack of β-alanine on the activated carbonyl group of **1** leads to formation of AMP and pantothenate (Scheme 1 A). Several crystal structures of *M. tuberculosis* pantothenate synthetase in complex with substrates and products bound have been solved.[13,14] These structures provide informative snapshots of the enzyme in action during catalysis.[14] Despite the extensive structural and mechanistic information available, no inhibitors of *M. tuberculosis* pantothenate synthetase have been developed to date by using rational drug design. Nevertheless, increasing interest in pantothenate synthetase as an antitubercular target has led to the recent identification of potential inhibitors from high-throughput screens.[15,16]

Reaction intermediate **1** is assumed to bind tightly in the active site. Consequently, it was expected that nonreactive analogues of **1** would be potent inhibitors of the enzyme. This approach has precedence in the inhibition of aminoacyl-tRNA synthetases, which are structurally related to pantothenate synthetase, by sulfamoyl adenylate analogues that mimic the aminoacyl adenylate intermediate.[17,18] A similar strategy has been employed to develop potent inhibitors of the adenylation enzyme MbtA, which catalyses the first step in the biosynthetic pathway to the siderophore mycobactin in *M. tuberculosis*. A sulfamoyl adenylate mimic of the salicyl adenylate intermediate in the MbtA reaction exhibited nanomolar potency in vitro and showed activity against *M. tuberculosis* in cell-based assays at low micromolar concentrations.[19–21]

[a] *Dr. A. Ciulli, Dr. D. E. Scott, M. Ando, Dr. F. Reyes, Dr. S. A. Saldanha, Dr. K. L. Tuck, Prof. C. Abell*
University Chemical Laboratory, University of Cambridge
Lensfield Road, Cambridge, CB2 1EW (UK)
Fax: (+44) 1223-336362
E-mail: ac313@cam.ac.uk
ca26@cam.ac.uk

[b] *Dr. D. Y. Chirgadze, Prof. Sir T. L. Blundell*
Department of Biochemistry, University of Cambridge
80 Tennis Court Road, Cambridge, CB2 1GA (UK)

[c] *M. Ando*
Present address: Medical Science Division
3rd Patent Examination Department (Japan) Patent Office 4–3
Kasumigaseki 3-chome, Chiyoda-ku, Tokyo 100–8915 (Japan)

[d] *Dr. F. Reyes*
Present address: Medicinal Chemistry Department, PharmaMar S.A.U.
Pol. Ind. La Mina Norte, Avenida de los Reyes 1
28770 Colmenar Viejo, Madrid (Spain)

[e] *Dr. S. A. Saldanha*
Present address: The Scripps Research Institute
Building 3377, 10550 North Torrey Pines Road
La Jolla, CA 92037 (USA)

[f] *Dr. K. L. Tuck*
Present address: School of Chemistry, Monash University
Clayton, Victoria 3800 (Australia)

Supporting information for this article is available on the WWW under http://www.chembiochem.org or from the author.

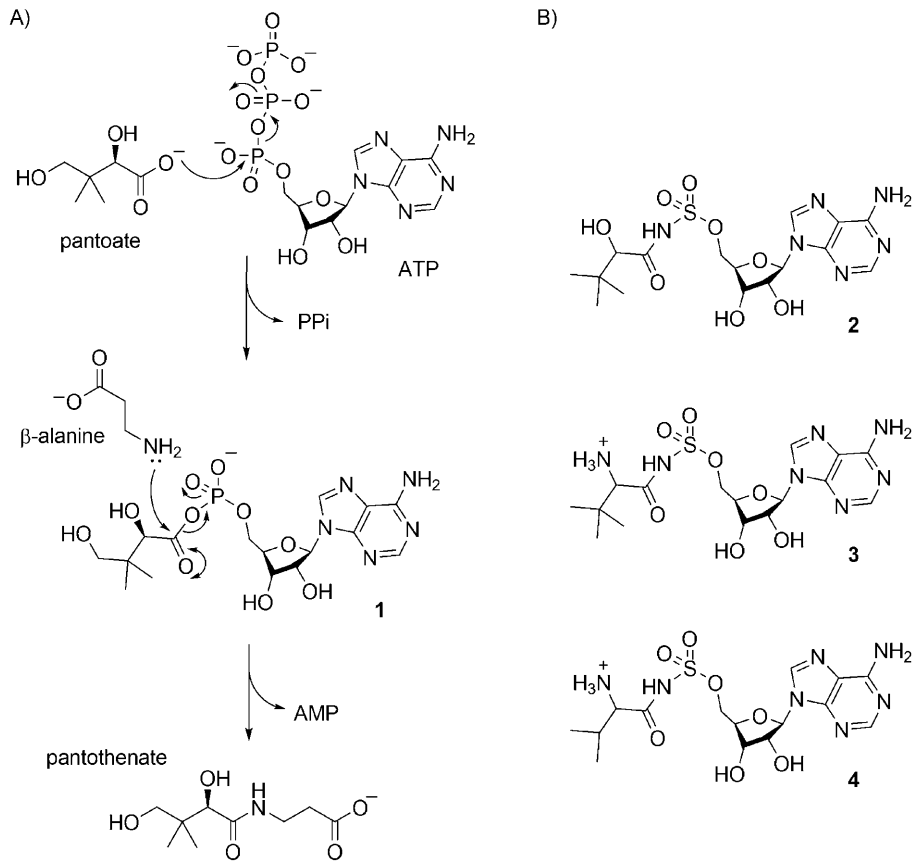

Scheme 1. A) Reaction catalyzed by pantothenate synthetase; the scheme shows the structure of pantoyl adenylate intermediate **1**. B) Structures of sulfamoyl analogues **2**–**4** used in this study.

Results and Discussion

In this paper, we report the high resolution crystal structures of *M. tuberculosis* pantothenate synthetase complexed with three sulfamoyl adenylate inhibitors that closely mimic the structure of the reaction intermediate **1** and the biophysical characterization of their binding to the enzyme using isothermal titration calorimetry (ITC), thermal denaturation assays and kinetic inhibition studies. The sulfamoyl adenylates **2**–**4** (Scheme 1 B) all lack the terminal hydroxyl of the pantoyl moiety found on **1,** which should prevent decomposition by lactonization.[22] Sulfamoyl **2** and **3** were synthesized as epimeric mixtures by coupling 2′,3′-protected adenosinesulfamate with appropriately activated carboxylic acid derivatives followed by deprotection under acidic conditions as previously described,[23] and **4** was prepared following a similar synthetic approach. Initially, the compounds were tested for activity against purified recombinant His_6-PS by using a spectrophotometric-coupled assay. The measured k_{cat} of His_6-PS (1.2 s^{-1}) is similar to that of the native enzyme (3.4 s^{-1}).[11,12,22] Full inhibition curves were obtained for all three compounds, and all were found to be competitive against ATP (Table 1). Compound **2**, which is structurally the most similar to intermediate **1**, was the most potent inhibitor within the series (K_i = 220 nM, Figure 1 A). Sulfamoyl **3** and **4** were less potent and exhibited K_i values of 4 and 18 μM, respectively (Table 1). To determine the thermodynamics of binding, the interaction of pantothenate synthetase with the inhibitors was characterized by using ITC (Table 1). An ITC experiment in which inhibitor **2** was titrated against His_6-PS is shown in Figure 1 B. The dissociation constant for **2** was 125 nM. The binding interaction was driven by a large apparent enthalpy ($\Delta H = -18.2$ kcal mol^{-1}), whereas the entropic term was unfavourable ($-T\Delta S =$ 8.8 kcal mol^{-1}). Inhibitors **3** and **4** exhibited weaker binding than **2** (see Figures S1–2 in the Supporting Information for ITC titrations). The K_d values for **3** and **4** were 1.0 and 2.7 μM, respectively. The enthalpies were favourable ($\Delta H = -17.8$ and -11.9 kcal mol^{-1}, respectively), and the entropic terms were unfavourable ($-T\Delta S = 9.6$ and 4.3 kcal mol^{-1}, respectively). By comparison, ATP bound more weakly than the inhibitors (K_d = 10 μM), but exhibited a similar thermodynamic footprint of binding with a large negative enthalpy ($\Delta H = -13.7$ kcal mol^{-1}) that overcomes an unfavourable entropic term ($-T\Delta S = 6.9$ kcal mol^{-1}). Finally, the stabilization of the enzyme by the inhibitors was monitored by using a thermal-shift assay (Figure S3 in the Supporting Information). Increases in T_m of 10.5, 7.5 and 6.5 °C were observed in the presence of 30 μM of **2**, 60 μM of **3** and 150 μM of **4**, respec-

Table 1. Summary of inhibition and biophysical data of inhibitors of *M. tuberculosis* pantothenate synthetase, and comparison with cofactor ATP.

	ATP	2	3	4
K_i [μM][a]	(K_m=320±80 μM)	0.22 ± 0.03 (C)[b]	4 ± 0.6 (C)[b]	18 ± 3 (C)[b]
K_d [μM][c]	10.3 ± 0.2	0.125 ± 0.008	0.96 ± 0.03	2.7 ± 0.1
ΔG [kcal mol^{-1}][c]	−6.81 ± 0.01	−9.43 ± 0.04	−8.22 ± 0.02	−7.61 ± 0.04
ΔH [kcal mol^{-1}][c]	−13.7 ± 0.1	−18.2 ± 0.1	−17.8 ± 0.1	−11.9 ± 0.4
$-T\Delta S$ [kcal mol^{-1}][c]	6.9 ± 0.1	8.8 ± 0.1	9.6 ± 0.1	4.3 ± 0.4
ΔT_m [°C][d]	6.0	10.5	7.5	6.5

[a] From kinetic assays at 25 °C. [b] C: competitive inhibition. [c] From ITC at 25 °C. [d] From thermal shift assay (T_m of His_6-PS: 38 °C).

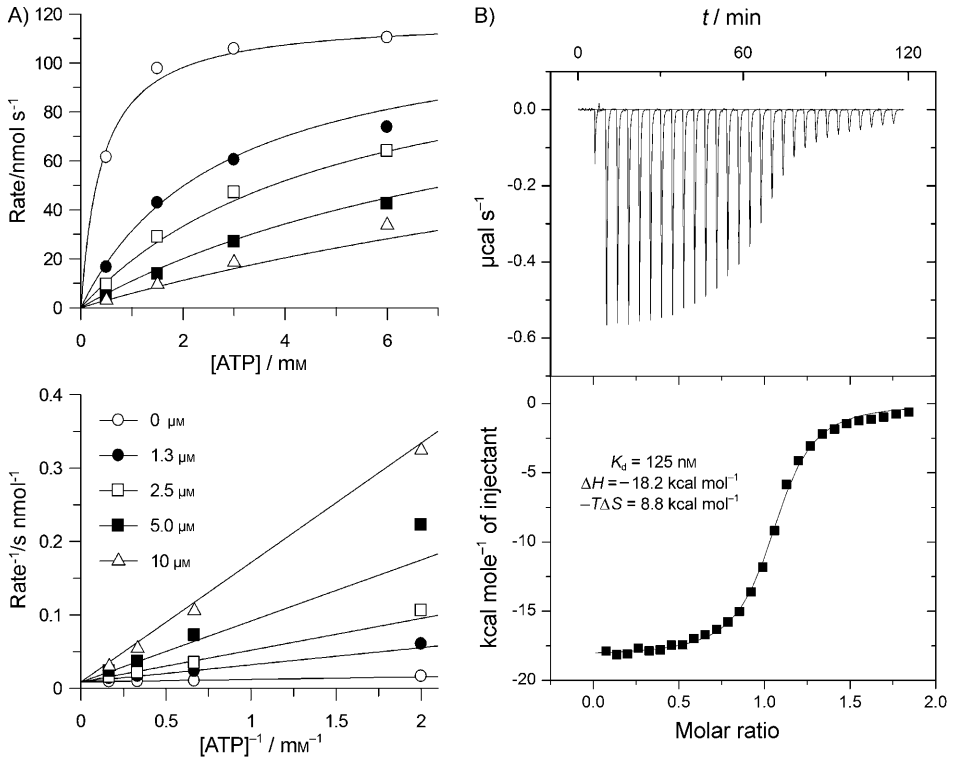

Figure 1. Inhibition and binding studies of *M. tuberculosis* pantothenate synthetase with sulfamoyl inhibitor **2**. A) Steady-state inhibition analysis of **2** versus ATP. The data were fitted to the equation for competitive inhibition and gave a K_i of 220 ± 30 nM. B) ITC analysis at 25 °C. Raw data for titration of 90 μM of **2** into 10 μM enzyme is shown in the top panel. Each peak corresponds to one injection, with an initial 3 μL injection followed by 27 × 10 μL injections. Integration of the data, which were corrected for the heat of dilution, is shown in the lower panel. The line represents the least-squares fit to a single-site binding model.

tively, compared to a ΔT_m of 6 °C shown in the presence of 500 μM ATP (Table 1).

Since the hydroxyl group of intermediate **1** is in the *R* configuration, the diastereoisomers of **2**–**4**, which have the same hydroxyl configuration, should presumably have greater affinity for pantothenate synthetase. To confirm this and gain detailed insight into their binding interactions at atomic level, we determined the crystal structures of all the enzyme–ligand complexes (see Table S2 for data collection and refinement statistics). First, we obtained crystals of the untagged enzyme that diffracted down to 1.5 Å of resolution. The protein crystals were then soaked with compounds (3–6 mM) for 16 h, and the structures of their complexes were solved to 1.80–2.05 Å of resolution. The overall structure of the pantothenate synthetase dimer in complex with **2** is shown in Figure 2A. The omit difference electron density ($F_o - F_c$) in the active site unambiguously identified the bound inhibitor as the diastereoisomer of **2**, the hydroxyl of which has the same *R* configuration as pantoyl adenylate **1** (Figure 2B and Figure S4A). Inhibitor **2** fits tightly in the active site cavity and makes extensive binding interactions (Figure 2C). The adenine group makes hydrogen bond contacts with the backbone amides of Val187 and Met195. Hydrogen bonds are also formed between the ribose hydroxyl groups and the Asp161 carboxylate and with the main chain atoms of Gly158 at the bottom of the active site cavity. The sulphonamide group interacts with the backbone amide of Met40 and the side chain of His44. The carbonyl and terminal hydroxyl groups make hydrogen bonds with conserved residues Gln72 and Gln164 at the pantoate binding site, and the terminal *tert*-butyl group binds in a hydrophobic pocket within this site defined by the side chains of Pro38, Met40, Val139, Val142, Val143 and Phe157 (Figure 2D). The binding mode is overall very similar with that of pantoyl adenylate intermediate **1**, and so are the key interactions formed with the enzyme (Figure S5). An ordered network of water molecules in the active site is found around the sulphonamide group of **2**. Notably, two water molecules appear to play an important role by mediating hydrogen bonds between the carboxylate moiety of Asp161 and the sulphonamide and carbonyl groups of **2** (Figure 2C). Interestingly, these water molecules are absent in the structure of the apoenzyme but are present in the structure with pantoyl adenylate bound. The crystal structures of **3** and **4** confirmed the binding mode and interactions observed for **2** (Figure S4). Inhibitors **3** and **4** bound so that their amine substituents pointed in the same direction as the hydroxyl of pantoyl adenylate and **2**, that is, in the same direction as the diastereoisomers with the *R* configuration at this position. Only one of the two waters described for the enzyme–**2** complex is present in the structure of the enzyme with **3** bound, whilst both water molecules are absent in the structure with **4** bound (Figure S4).

The trend in binding affinity, **2** ≫ **3** > **4** > ATP, is observed in both the inhibition and calorimetric data, and is supported by the thermal shift results (Table 1); it provides a strong rationale for structure-activity relationships within the inhibitor series. The changes in B-factors across the series, **2** ≪ **3** < **4** (Table S2), are significant given the comparable resolutions of the three liganded structures, and suggest that **2** is bound more tightly than **3** and **4**; this is consistent with the trend in affinities.

The high affinity of **2** is reflected by good binding interactions between the terminal hydroxyl group and the neutral side chains of Gln72 and Gln164. The hydroxyl group forms a hydrogen bond to the carbonyl group of Gln164 (acceptor functionality) and a second hydrogen bond to the amide nitrogen of Gln72 (donor functionality). Replacement of this hydroxyl group with an amine in **3** and **4** had a deleterious effect on

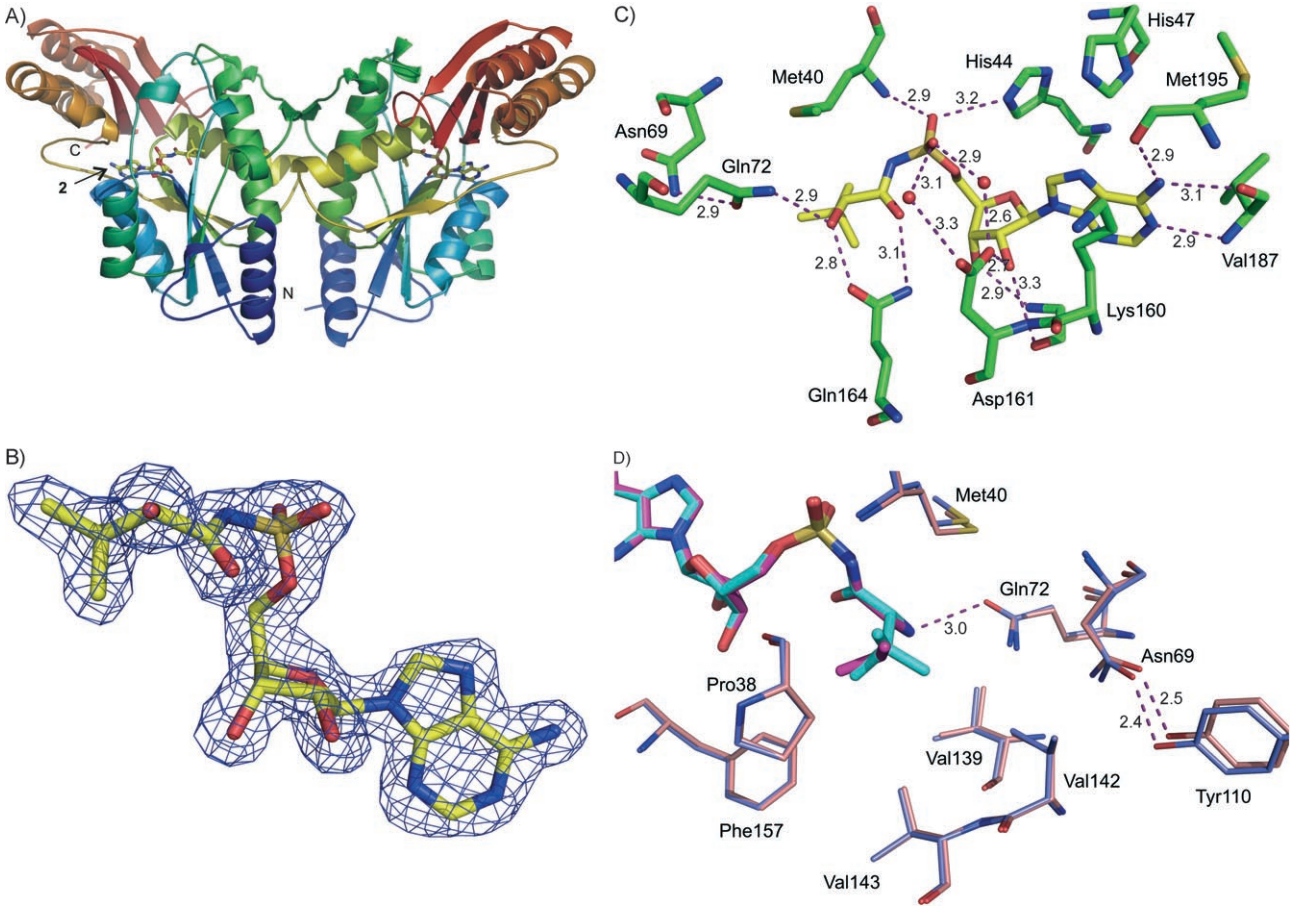

Figure 2. The crystal structure of *M. tuberculosis* pantothenate synthetase with inhibitor **2** bound, solved at 1.80 Å resolution. A) The side view of the ribbon diagram for the pantothenate synthetase dimer has a shape that resembles a butterfly. The inhibitor molecules (yellow carbons) mark the location of the active site in each subunit. B) The omit difference electron density ($F_o - F_c$) superimposed around **2** is shown in blue contoured at 3σ. C) The detailed binding interactions of **2** in the active site of one subunit. The inhibitor is shown as sticks with yellow carbons. Key protein residues are shown with carbon atoms in green, nitrogen in blue, oxygen in red and sulfur in orange. Hydrogen bonds are indicated with dark purple dashed lines and H-bond distances are given. D) Superposition of the enzyme structures in complex with **3** (cyan carbon) and **4** (magenta carbons), showing details of the pantoate binding site. Key protein residues are shown with purple (PS–**3**) and pink (PS–**4**) carbons. The figures were generated and rendered by using Pymol v.0.99.[29]

the binding affinity, which can be rationalized in structural terms. The amine group becomes faced by acceptor functionalities from both Gln72 and Gln164. A third potential hydrogen bond appears not to be formed, as the closest acceptor group is from a water molecule that is 3.5 and 4 Å away in the liganded complexes of **3** and **4**, respectively. In order to accommodate this new hydrogen bond pattern around the amine group of the inhibitors, a flip in the orientation of the carboxamide group of Gln72 is required; this results in disruption of an internal hydrogen bond between Gln72 and Asn69 (Figure 2D). This interaction is part of a hydrogen bond network that involves Gln72, Asn69 and Tyr110 (Figure 2D), and is seen in all other crystal structures of *M. tuberculosis* pantothenate synthetase. It is noteworthy that these three residues are entirely conserved across bacterial pantothenate synthetases, and that mutational studies have identified both Asn69 and Gln72 as being important for enzyme activity.[22] A second structural explanation for the loss of affinity going from **2** to **3** and **4** is that at physiological pH the amine groups of **3** and **4** will likely be protonated. The NH_3^+ group is entirely buried within the enzyme active site and its positive charge appears to be poorly accommodated due to the lack of acidic residues close by. Finally, replacement of the terminal *tert*-butyl with an *iso*-propyl group in **4** resulted in a further reduction of binding affinity and inhibition potency, although the affinity loss relative to **3** (~threefold) was smaller than the effect observed between **2** to **3** (~tenfold). Removal of a terminal methyl group leaves a void in the structure and results in loss of hydrophobic contacts with Val139, Val142, Val143 in the pocket. There is no evidence of a collapse in the structure as all the residues present in this hydrophobic pocket superpose very well (Figure 2D).

In conclusion, we have reported the binding, inhibition and cocrystal structures of three inhibitors of *M. tuberculosis* pantothenate synthetase that mimic the structure of the adenylate intermediate in the enzyme catalytic mechanism. The most potent compound exhibited dissociation and inhibition constants in the nanomolar range and is now being tested for activity in a cell-based assay against *M. tuberculosis*. The binding modes of the inhibitors determined by X-ray crystallography

were found to recapitulate that of the reaction intermediate pantoyl adenylate. The structural elucidation of the binding interactions has identified key features within the pantoate pocket that determine high affinity, such as the effective hydrogen bonding with conserved residues Gln72 and Gln164, as well as the presence of water molecules that mediate interaction of the sulphonamide group in the active site. Furthermore, the compounds described here will be useful tools for designing inhibitors of *M. tuberculosis* pantothenate synthetase through rational design and fragment-based approaches,[24] with the aim to ultimately generate new classes of lead compounds against TB.

Experimental Section

Expression, purification, characterization and tag removal of His_6-tagged pantothenate synthetase: The plasmid pET30a encoding pantothenate synthetase from *M. tuberculosis* was kindly provided by Dr. Wang, University of California, Los Angeles. The protein was expressed and purified as previously described.[13,14] The detailed procedures for protein expression, purification and characterization of the protein and enterokinase cleavage of the tag are in the Supporting Information.

Enzyme kinetic assay: Pantothenate synthetase activity was assayed as described in the Supporting Information.

Isothermal titration calorimetry: ITC experiments were performed on a VP-ITC instrument from Microcal Inc. (Northampton, MA, USA), at 25 °C. His_6-PS was buffer-exchanged in HEPES-HCl (50 mM, pH 7.6) containing NaCl (50 mM) and $MgCl_2$ (5 mM) as described in the Supporting Information. Ligands were dissolved in the same buffer and their concentrations were determined by UV spectrophotometry by using extinction coefficient $\varepsilon = 15\,400\ M^{-1}cm^{-1}$ at 259 nm. To determine ATP binding parameters, enzyme (50 μM) was loaded in the sample cell (1.345 mL). Typically, 35×8.0 μL injections of 8 s duration were made at 3–4 min intervals from a 300 μL syringe that rotated at 300 rpm and loaded with a solution of ATP (500 μM). This was performed as a control titration to allow an independent measure of the concentration of active sites based on the stoichiometry ($n = 1$). To determine the thermodynamic parameters of inhibitor binding, 27×10.0 μL injections of inhibitor solutions (90–210 μM) were made in to a sample cell that contained enzyme (10–15 μM). In all cases, an initial injection of ligand (2 μL) was made and discarded during data analysis. The heat change accompanying the titration was recorded as differential power by the instrument and determined by integration of the peak obtained. Titrations of ligand to buffer were performed to allow base-line corrections. The corrected heat change was then fitted by using nonlinear least-squares minimization to obtain the dissociation constants, K_d, the enthalpy, ΔH, and the stoichiometry, n. The enthalpy of ionization of HEPES buffer used in the ITC titrations is 4.9 kcal mol^{-1}, and thus any contributions to the observed ΔH that arose from protonation effects should haven been small relative to the ΔH of binding.

Thermal shift assay: The fluorescent dye, Sypro Orange, was used to monitor protein unfolding. Sypro Orange is an environmentally sensitive dye that binds preferentially to the unfolded state of a protein; this resulted in an increase in fluorescence, which was used to monitor the unfolding transition.[24] The thermal-shift assay was conducted by using the iCycler iQ real time detection system (Bio-Rad). Solutions (100 μL) in each of the 8-tube iCycler iQ PCR strips contained His_6-PS (final concentration 4 μM), Sypro Orange (2.5×), HEPES-HCl (50 mM, pH 7.6), NaCl (50 mM) and MgCl2 (5 mM). The final compound concentration was 30, 60, 150 and 500 μM for **2**, **3**, **4** and ATP, respectively. The samples were warmed in the thermal cycler from 25 to 90 °C with a heating rate of 0.5 °C min^{-1}, and the fluorescence was monitored continuously with Ex/Em at 490/530 nm.

Protein crystallography: Crystallization was carried out as previously described.[13,14] Briefly, the His_6-tag of the recombinant enzyme was cleaved by enterokinase (Supporting Information) and the purified, cleaved protein was exchanged into HEPES (5 mM, pH 7.6) containing NaCl (10 mM) by three cycles of dilution/concentration, and then concentrated to ~20 mg mL^{-1}. Crystal trials were carried out by using the hanging drop vapour-diffusion technique with a protein concentration of 10–20 mg mL^{-1}. In each drop, protein solution (1 μL) was mixed with an equal volume of well solution. Diffraction quality single crystals grew over 2–3 days from drops set up with well solutions that contained PEG3000 (12–14%), Li_2SO_4 (100–150 mM), and imidazole (100 mM) at pH 8.0 and 20 °C, in the presence of ethanol (2–4%, *v/v*), glycerol (5–10%, *v/v*) and $MgCl_2$ (20 mM) as additives. All soaking experiments were carried out, overnight (~16 h) by adding 1.5 μL of soak solutions that contained the inhibitors. For inhibitor **2**, the final soak solution consisted of PEG3000 (12%), Li_2SO_4 (150 mM), imidazole buffer (0.1 M, pH 8.0), ethanol (2%), glycerol (10%) and $MgCl_2$ (20 mM), and contained **2** (2.5 mM) in DMSO (5%, *v/v*). For inhibitors **3** and **4**, the final soak solution consisted of PEG3000 (12%), imidazole buffer (0.1 M, pH 8.0), ethanol (4%) and glycerol (10%), and contained inhibitor (6 mM) in DMSO (3%, *v/v*).

X-ray data were collected at European Synchrotron Radiation Facility synchrotron, beam station ID29 (Grenoble, France). The structure of apo pantothenate synthetase was solved by molecular replacement by using AMoRe, from the CCP4 suite,[25] with the structure of pantothenate synthetase (PDB ID: 1mop[13]) as the molecular replacement search probe. The structure was refined by using successive rounds of manual rebuilding in Coot 0.0.33[26] and maximum likelihood refinement with Refmac 5 from the CCP4 suite.[27,28] The structure of the apo enzyme was used to calculate phases for the data sets of the complexes with inhibitors by maximum likelihood refinement by using Refmac 5 into the new data sets. Data collection and final refinement statistics for all the refined coordinate sets are presented in Table S2.

Accession codes: The atomic coordinates and structure factors for the apoenzyme and enzyme–ligand complexes have been deposited in the Protein Data Bank with the following ID codes: 3cov (apo-PS), 3cow (PS–**2**), 3coy (PS–**3**) and 3coz (PS–**4**).

Acknowledgements

This work was supported by the UK Biotechnology and Biological Sciences Research Council. We also wish to thank Homerton College (A.C.), the UK Engineering and Physical Sciences Research Council (D.E.S.), the Spanish Ministry of Education and Culture (F.R.), the Japan Patent Office (M.A.), and the Wellcome Trust (D.Y.C.) for funding. We are grateful to Dr. Shuishu Wang (University of California, Los Angeles) for a gift of the plasmid DNA encoding M. tuberculosis panC.

Keywords: drug design · enzyme inhibition · isothermal titration calorimetry · protein structures · tuberculosis

[1] E. L. Corbett, C. J. Watt, N. Walker, D. Maher, B. G. Williams, M. C. Raviglione, C. Dye, *Arch. Intern. Med.* **2003**, *163*, 1009–1021.
[2] S. T. Cole, K. D. Eisenach, D. N. McMurray, W. R. Jacobs, *Tuberculosis and the Tubercle Bacillus* (Eds.: S. T. Cole, K. D. Eisenach, D. N. McMurray, W. R. Jacobs), ASM, Washington, D.C. **2005**, pp. 1–584.
[3] World Health Organization **2008**, *Global Tuberculosis Control: Surveillance Planning Financing*, Geneva WHO/HTM/TB/2008.393.
[4] S. Nwaka, A. Hudson, *Nat. Rev. Drug Discovery* **2006**, *5*, 941–955.
[5] M. E. Webb, A. G. Smith, C. Abell, *Nat. Prod. Rep.* **2004**, *21*, 695–721.
[6] K. Mdluli, M. Spigelman, *Curr. Opin. Pharmacol.* **2006**, *6*, 459–467.
[7] V. K. Sambandamurthy, X. J. Wang, B. Chen, R. G. Russell, S. Derrick, F. M. Collins, S. L. Morris, W. R. Jacobs, *Nat. Med.* **2002**, *8*, 1171–1174.
[8] V. K. Sambandamurthy, S. C. Derrick, T. Hsu, B. Chen, M. H. Larsen, K. V. Jalapathy, M. Chen, J. Kim, S. A. Porcelli, J. Chan, S. L. Morris, W. R. Jacobs, Jr., *Vaccine* **2006**, *24*, 6309–6320.
[9] S. Y. Gerdes, M. D. Scholle, M. D'Souza, A. Bernal, M. V. Baev, M. Farrell, O. V. Kurnasov, M. D. Daugherty, F. Mseeh, B. M. Polanuyer, J. W. Campbell, S. Anantha, K. Y. Shatalin, S. A. K. Chowdhury, M. Y. Fonstein, A. L. Osterman, *J. Bacteriol.* **2002**, *184*, 4555–4572.
[10] D. J. Murphy, J. R. Brown, *BMC Infect. Dis.* **2007**, *7*, 84.
[11] R. Zheng, J. S. Blanchard, *Biochemistry* **2001**, *40*, 12904–12912.
[12] L. K. Williams, R. Zheng, J. S. Blanchard, F. M. Raushel, *Biochemistry* **2003**, *42*, 5108–5113.
[13] S. Wang, D. Eisenberg, *Protein Sci.* **2003**, *12*, 1097–1108.
[14] S. Wang, D. Eisenberg, *Biochemistry* **2006**, *45*, 1554–1561.
[15] E. L. White, K. Southworth, L. Ross, S. Cooley, R. B. Gill, M. I. Sosa, A. Manouvakhova, L. Rasmussen, C. Goulding, D. Eisenberg, T. M. Fletcher, III, *J. Biomol. Screening* **2007**, *12*, 100–105.
[16] S. Velaparthi, M. Brunsteiner, R. Uddin, B. Wan, S. G. Franzblau, P. A. Petukhov, *J. Med. Chem.* **2008**, *51*, 1999–2002.
[17] H. Belrhali, A. Yaremchuk, M. Tukalo, K. Larsen, C. Berthet-Colominas, R. Leberman, B. Beijer, B. Sproat, J. Als-Nielsen, G. Grubel, J. F. Legrand, M. Lehmann, S. Cusack, *Science* **1994**, *263*, 1432–1436.
[18] S. Bernier, P. M. Akochy, J. Lapointe, R. Chenevert, *Bioorg. Med. Chem.* **2005**, *13*, 69–75.
[19] J. A. Ferreras, J. S. Ryu, F. Di Lello, D. S. Tan, L. E. Quadri, *Nat. Chem. Biol.* **2005**, *1*, 29–32.
[20] R. V. Somu, H. Boshoff, C. H. Qiao, E. M. Bennett, C. E. Barry, C. C. Aldrich, *J. Med. Chem.* **2006**, *49*, 31–34.
[21] R. V. Somu, D. J. Wilson, E. M. Bennett, H. I. Boshoff, L. Celia, B. J. Beck, C. E. Barry, III, C. C. Aldrich, *J. Med. Chem.* **2006**, *49*, 7623–7635.
[22] R. Zheng, T. K. Dam, C. F. Brewer, J. S. Blanchard, *Biochemistry* **2004**, *43*, 7171–7178.
[23] K. L. Tuck, S. A. Saldanha, L. M. Birch, A. G. Smith, C. Abell, *Org. Biomol. Chem.* **2006**, *4*, 3598–3610.
[24] A. Ciulli, C. Abell, *Curr. Opin. Biotechnol.* **2007**, *18*, 489–496.
[25] J. Navaza, *Acta Crystallogr. Sect. D* **2001**, *57*, 1367–1372.
[26] P. Emsley, K. Cowtan, *Acta Crystallogr. Sect. D* **2004**, *60*, 2126–2132.
[27] G. N. Murshudov, A. A. Vagin, E. J. Dodson, *Acta Crystallogr. Sect. D* **1997**, *53*, 240–255.
[28] Collaborative Computational Project, Number 4, *Acta Crystallogr. D Biol. Crystallogr.* **1994**, *50*, 760–763.
[29] W. L. Delano, *The PyMOL Molecular Graphics System*, v0.99, **2002**. DeLano Scientific, San Carlos, CA (USA).

Received: June 27, 2008
Published online on September 26, 2008

